Available online at www.sciencedirect.com
SCIENCE DIRECT®
Journal of Photochemistry and Photobiology A: Chemistry 162 (2004) 615–623
Journal of Photochemistry and Photobiology A:Chemistry
www.elsevier.com/locate/jphotochem

# Photodynamic action of damnacanthal and nordamnacanthal

M. Rajendran [a], J. Johnson Inbaraj [b], R. Gandhidasan [c], R. Murugesan [c,*]

[a] *Department of Chemistry, NMSSVN College, Madurai 625 019, Tamil Nadu, India*
[b] *Laboratory of Pharmacology and Chemistry, NIEHS, Research Triangle Park, NC, USA*
[c] *School of Chemistry, Madurai Kamaraj University, Madurai 625 021, Tamil Nadu, India*

**Abstract**

Photodynamic properties of two anthraquinones, damnacanthal (DAM) and nordamnacanthal (NDAM) are studied. Photogeneration of singlet oxygen is monitored by both optical, and EPR methods. In comparison with rose bengal ($\Phi^1O_2$ for RB = 0.76), singlet oxygen generating efficiencies of DAM and NDAM are determined to be 0.29 and 0.10, respectively. Rate of RNO bleaching is found to be retarded by specific $^1O_2$ quenchers such as DABCO and $NaN_3$, confirming the involvement of $^1O_2$ as an active intermediate. Photolysis of DAM and NDAM in DMSO, in the presence of spin trap 5,5-dimethyl-1-pyrroline-*N*-oxide (DMPO) generates 12-line EPR spectra, characteristic of $O_2^{\bullet-}$ adduct. Photogeneration of $O_2^{\bullet-}$ is also monitored by optical spectroscopy using SOD inhibitable cytochrome *c* reduction assay. Our results indicate that DAM possesses high ability to generate reactive oxygen species. Both Type I and Type II paths are involved in the photosensitisation of DAM as well as NDAM. The quantum mechanically calculated lowest unoccupied molecular orbital (LUMO) energies of DAM and NDAM are correlated with the experimental redox potential.


*Keywords:* 5,5-Dimethyl-1-pyrroline-*N*-oxide; Damnacanthal; Singlet oxygen; Superoxide anion radical; Molecular modelling

## 1. Introduction

Damnacanthal (DAM), nordamnacanthal (NDAM) comprise of a general class of anthraquinone derivatives. These naturally occurring quinones are present in the heartwood of *Morinda tinctoria* Roxb. [1]. DAM has some unique chemical and biological properties [2–4]. It shows inhibitory effect towards tyrosine kinases such as Lck, Src, Lyn and EGF receptor of DAM [5]. The effect of DAM on intracellular Ca (2+) mobilisation has been demonstrated in cultured bovine coronary endothelial cells [6]. The specific inhibitory effect of DAM on tyrosine kinase is used to study of structural basis of selectivity and potency [7]. DAM shows an intensive inhibitory effect against DNA topoisomerase II (IC 50: 20 μg/ml) [8].

The stimulatory effect of DAM on photodynamic process has been studied on both phosphorylated extracellular signal-regulated kinases and stress-activated protein kinases [9]. This effect is strongly light-dependent; therefore, studies on photodynamic effects of DAM and structurally related NDAM are of considerable interest. Photosensitisers DAM and NDAM are excited from ground state (S) to a triplet ($^3S$) by the absorption of light. In Type I reactions, $^3S$ participates in electron transfer to $O_2$ to form superoxide anion radicals, whereas in Type II reactions, $^3S$ can transfer its excitation energy to $O_2$ to form singlet oxygen. The aim of the present study is to examine the photophysical properties of both DAM and NDAM. The present study reports the photogeneration of both $^1O_2$ and $O_2^{\bullet-}$ by DAM and NDAM. The effect of electron donors such as ethylenediaminetetraacetic acid (EDTA) and reduced nicotinamide adenine dinucleotide (NADH) on the efficiencies of production of reactive oxygen species (ROS) by these quinones is also presented. A semi-empirical quantum mechanical calculation is also made to compute the HOMO and LUMO energies.

## 2. Materials and methods

### 2.1. Chemicals

DAM and NDAM were received as gift from the Department of Natural Product Chemistry (NPC), Madurai Kamaraj University, India, and used as received. The structures and UV-Vis spectra of DAM and NDAM in phosphate buffer (pH 7.4) are given in Fig. 1.

Superoxide dismutase (SOD), catalase and cytochrome *c* were purchased from Sigma Chemical Co., while reduced

* Corresponding author. Tel.: +91-452-858246; fax: +91-452-2459105.
*E-mail address:* rammurugesan@yahoo.com (R. Murugesan).

1010-6030/$ – see front matter © 2004 Elsevier B.V. All rights reserved.
doi:10.1016/S1010-6030(03)00415-5

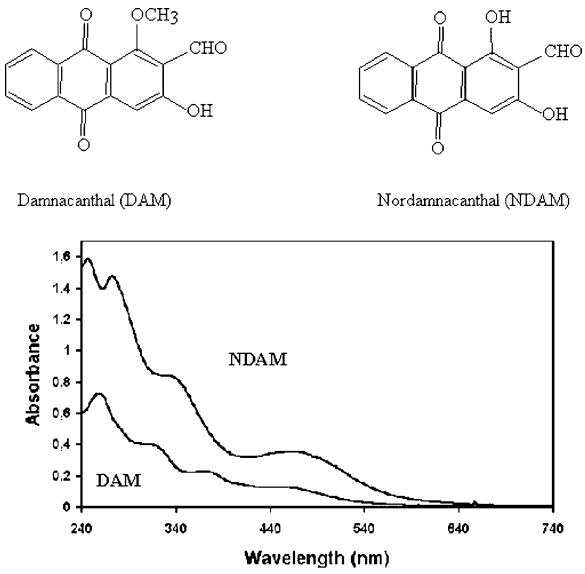


Fig. 1. Chemical structures and UV-Vis spectra of DAM and NDAM. UV-Vis spectra were recorded in phosphate buffer (pH 7.4) by DAM ($\lambda_{max}$ at 260, 317, 371, 457 nm) and NDAM ($\lambda_{max}$ at 268, 345, 457 nm).

NADH was obtained from Boehringer Mannheim. Dimethyl sulphoxide (HPLC grade) was procured from Qualigens Fine Chemicals, India. *N*,*N*-Dimethyl-4-nitrosoaniline (RNO), 1,4-diazabicyclo[2,2,2]octane (DABCO) and rose bengal (RB) were obtained from Aldrich Chemical Co., Milwaukee, WI. Perinaphthenone (PN; Aldrich) was used as a standard for the determination of the singlet oxygen quantum yields. The spin trap 5,5-dimethyl-1-pyrroline-*N*-oxide (DMPO) was obtained from Aldrich and was purified by activated charcoal [10]. 2,2,6,6-Tetramethyl piperidinol (TEMPL) was obtained from Merck, India. Imidazole, EDTA and sodium azide were purchased from S.D. Fine Chemicals, India. Imidazole was used after repeated crystallisation from doubly distilled water. All other compounds were used as received.

### 2.2. Light source

Light source used for irradiation was a 150 W xenon lamp. A filter combination of 10 cm potassium iodide solution (1 g in 100 ml) and 1 cm pyridine was used to cut off below 300 nm and achieve a spectral window of 300–700 nm. The irradiation was generally carried out in an open cuvette, in equilibrium with the atmosphere. The reaction mixture in a quartz cuvette, placed at a distance of 12 cm from the light source was continuously stirred during irradiation.

### 2.3. Detection of singlet oxygen

The singlet oxygen generating efficiencies of DAM and NDAM were measured by RNO bleaching assay, chemiluminescence and EPR methods. Photoexcitation of the sensitiser generates $^1O_2$, which bleaches RNO and the bleaching can be monitored spectrophotometrically at 440 nm [11]. The sensitiser was exposed to light in the presence of imidazole (10 mM) and RNO (50 mM) in a phosphate buffer (pH 7.4). Shimadzu UV-Vis spectrometer (UV-160) as well as Specord S100 UV-Vis spectrometer Analytik Jena AG, Jena, Germany, were used for optical measurements. The interference of $O_2^{\bullet -}$ and $H_2O_2$ on RNO bleaching was removed by the addition of SOD and catalase, respectively.

The rate of disappearance of quencher (A) obeys the following equation [12]:

$$-\frac{d[A]}{dt} = (I_{ab}\Phi^1O_2)\frac{K_r[A]}{K_d}$$

where $K_r$ is the rate constant for chemical quenching, $K_d$ the rate constant for deactivation of $^1O_2$ by the solvent, and $I_{ab}$ the intensity of light absorbed by the sensitiser. The slope of the first order plot is $I_{ab}\Phi^1O_2(K_r/K_d)$. The slope was calculated by curve fitting the experimental data. The quantum yield for $^1O_2$ generation of DAM and NDAM was determined based on the relative rates of RNO bleaching, under identical conditions, by reference to singlet oxygen generator RB. Corrections were made for molar absorption and photon energy [13]. $^1O_2$ quantum yield for RB is taken as 0.76 [14]. The details of the calculation is presented elsewhere [15].

The detection of $^1O_2$ by EPR was also used as an alternative method to determine the photogeneration of $^1O_2$ by DAM and NDAM [16,17]. EPR-TEMPL experiment was carried out for RB, DAM and NDAM under identical conditions. The reaction mixture (1 ml) containing 0.02 M TEMPL and 0.1 mM quinones in DMSO was irradiated and the increase in EPR signal intensity was followed as a function of time. TEMPOL, a stable nitroxide free radical, formed as a result of oxidation of TEMPL by $^1O_2$ shows a three line EPR spectrum. The formation of EPR signal intensity of TEMPOL was not observed in dark. EPR spectra were obtained with a JEOL JES-TE100 ESR spectrometer at room temperature. Samples were injected into gas-permeable Teflon capillary tube (0.8 mm inside diameter, 0.5 mm wall thickness) which was folded and inserted into a narrow quartz tube and placed in the EPR cavity for measurements [18,19].

### 2.4. Phosphorescence method

Phosphorescence spectra were recorded on an SLM SPC 823-SMC 220 spectrofluorimeter (SLM Instruments, Urbana, IL). Singlet oxygen phosphorescence was detected as described by Hall and Chignell [20]. Photosensitised production of $^1O_2$ from DAM and NDAM was calculated from its characteristic infrared (IR) phosphorescence at 1270 nm in acetonitrile. Singlet oxygen phosphorescence was measured as described elsewhere [21]. PN was used as standard for the determinations of the singlet oxygen quantum yields. The $^1O_2$ phosphorescence spectra were recorded over the range of 1200–1300 nm. The integrated areas of the $^1O_2$

phosphorescence spectra for each compound were corrected for the number of photons absorbed over the appropriate wavelengths and normalised to the same number of absorbed photons at the excitation wavelength [20].

### 2.5. Detection of superoxide anion

SOD inhibitable cytochrome *c* reduction method [22] was used to measure the superoxide generating efficiencies of the quinones. Solutions of photosensitiser were illuminated in the presence of ferricytochrome *c* in 50 mM phosphate buffer (pH 7.4) and the reduction was monitored, spectrophotometrically, at 550 nm, using $\Delta\varepsilon_{550} = 20\,000\,M^{-1}\,cm^{-1}$ for the reduced–oxidised cytochrome *c* [23].

EPR spin trapping method was also used for the detection of $O_2^{\bullet -}$ [24,25]. Solution of quinone (0.2 mM) and DMPO (100 mM) in DMSO, placed in a quartz cuvette, was continuously stirred using a magnetic stirrer during irradiation. Irradiated solution was drawn into a gas-permeable Teflon capillary tube (0.8 mm inside diameter, 0.5 mm wall thickness). The Teflon tube was folded, inserted into a narrow quartz tube, and placed in the EPR cavity. The microwave power was 2 mW and modulation amplitude was kept at 0.5 G. The spectral identification was confirmed by independently simulating the spectra with known hyperfine-coupling constant (hfcc) and comparing them with the experimentally obtained EPR spectrum. To simulate the EPR spectra, a BASIC computer program was used. The output from this program was plotted to get the simulated spectra.

### 2.6. Cyclic voltammetry

Redox potentials of quinones were investigated by using the electrochemical analyser, BAS 50A. The cell consists of a three-electrode assembly of glassy carbon electrode (working), platinum electrode (auxiliary) and Ag/AgCl (reference) electrode. Glassy carbon was resurfaced with alumina. Solutions of quinone (2 mg; 5 ml of acetonitrile) were prepared in HPLC grade acetronitrile containing 0.05 M tetrabutylammonium perchlorate (TBAP), as supporting electrolyte. Quinone solutions were deoxygenated for 10 min with nitrogen gas, prior to measurement. All potentials are reported against Ag/AgCl, unless otherwise mentioned.

### 2.7. Computational chemistry

To assess the effects of electron-donating substituents in the side chain of the anthraquinones (DAM and NDAM) semi-empirical quantum mechanical calculations were performed using Argus computer program version 3.0 [26]. This program supports QM/MM and QM/MMpol hybrid methods with different semi-empirical Hamiltonians [27,28]. In the present study, the properties of molecular orbital and atomic charges were predicted by using ZINDO/RHF (Restricted Hartree–Fock) semi-empirical Hamiltonial of Zerner et al. [29]. The heats of formation of neutral closed-shell anthraquinones were computed by using AM1 Hamiltonian. All molecular modeling calculations were performed on an MS-Windows 98 workstation.

## 3. Results and discussion

### 3.1. Generation of $^1O_2$

Bleaching of RNO as a function of irradiation time by DAM, NDAM and RB is shown in Fig. 2. The ratio of slopes of RB to each sensitiser was corrected for molar absorption and photon energy to obtain the singlet oxygen generating efficiencies of quinones. The singlet oxygen yields thus evaluated are 0.29 and 0.10 for DAM and NDAM, respectively.

To confirm the role of $^1O_2$ in bleaching of RNO, experiments were carried out in the presence of specific singlet oxygen quenchers such as DABCO and sodium azide (Fig. 3). The RNO bleaching rate constants in the presence of imidazole (10 mM) ($2 \times 10^7\,M^{-1}\,s^{-1}$) and DABCO (10 mM) ($1.5 \times 10^7\,M^{-1}\,s^{-1}$) are comparable [30]. Hence the rate of RNO bleaching should be reduced to 50% if equal concentration of imidazole and DABCO are used. In the present study the experiments were carried out in the presence of 10 mM imidazole and 5 mM DABCO. Hence bleaching rate was decreased by about 25% (0.05), when compared to the rate of RNO bleaching in the absence of DABCO. Similarly sodium azide, another singlet oxygen quencher also was used. The concentrations of sodium azide and imidazole used were 0.1 and 10 mM, respectively. At these concentrations, it was found that the RNO bleaching was inhibited by 50% (0.03). These results confirm the generation of $^1O_2$ during photodynamic process [30,31]. However, it is pointed out that the optical RNO bleaching method has a limitation, if compounds and RNO have same wavelength maxima. Hence another technique, the EPR method was used to study $^1O_2$ yield.

The generation of $^1O_2$ in photodynamic process was further confirmed by EPR method. In EPR technique the problems related to optical study are eliminated. The EPR spectrum of three equally intense lines, characteristic of TEMPOL nitroxide radical, was observed when the aerated solutions of DAM or NDAM and TEMPL in DMSO were irradiated at room temperature. The hfcc ($A_N = 15.7$ G) was found to be identical with those of the authentic TEMPOL sample. EPR signal intensity of TEMPOL was found to increase with increase of irradiation time as shown in Fig. 4. Under the same condition RB also showed the formation of TEMPOL. The rates of formation of TEMPOL by DAM and NDAM are parallel to their $^1O_2$ generating quantum yields. The relative $^1O_2$ generating ratios of RB, DAM and NDAM were determined to be 1:0.35:0.14, respectively. These ratios are comparable to the values determined by the RNO bleaching method. Control experiments indicated that sensitiser, oxygen and light were all essential for the

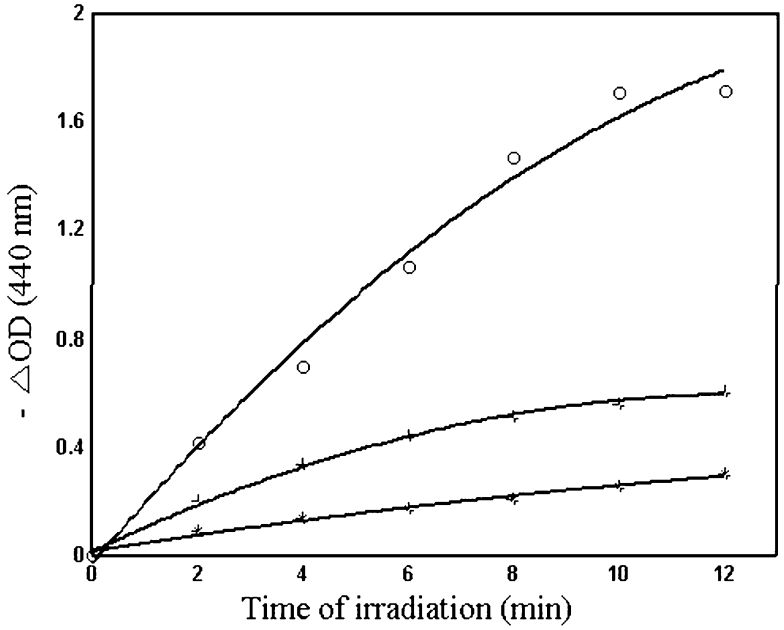


Fig. 2. Photosensitised RNO bleaching measured at 440 nm in the presence of imidazole (10 mm) in 50 mM phosphate buffer (pH 7.4) with RB (○), DAM (+) and NDAM (∗) as a function of illumination time.

production of TEMPOL, indicating that the formation of the nitroxide radical is a photodynamic process. The generation of $^1O_2$ during photoirradiation was further confirmed by studying the effect of sodium azide. The EPR signal intensity of TEMPOL was suppressed by $^1O_2$ quencher, azide, confirming the formation of $^1O_2$ (Fig. 4).

Singlet oxygen is generally formed through energy transfer from the excited triplet of the sensitiser to the ground state of dissolved molecular oxygen. PN is an efficient singlet oxygen sensitiser with quantum yield close to unity in most solvent [32]. For the compounds DAM and NDAM, in aqueous media the phosphorescence from $^1O_2$ was too weak to be detected. Hence the PN, DAM and NDAM are measured in acetonitrile. The singlet oxygen phosphorescence spectra for DAM, NDAM and PN in acetonitrile are shown in Fig. 5. The observed phosphorescence of DAM and NDAM clearly indicate that triplet states are populated under irradiation. The lifetime of phosphorescence is

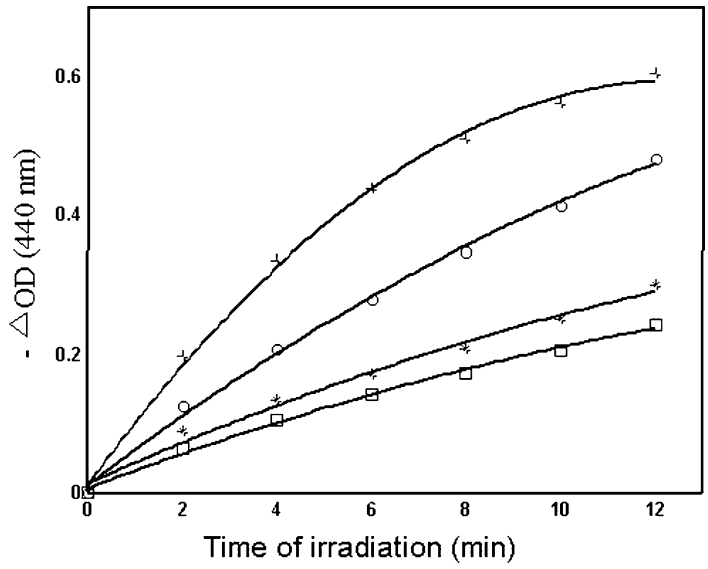


Fig. 3. Photosensitised RNO bleaching measured at 440 nm in the presence of imidazole (10 mM) in 50 mM phosphate buffer (pH 7.4) with DAM (+) and NDAM (∗) as a function of illumination time. Inhibition of photosensitised RNO bleaching by DAM in the presence of 0.1 mM sodium azide (□) and 5 mM DABCO (○).

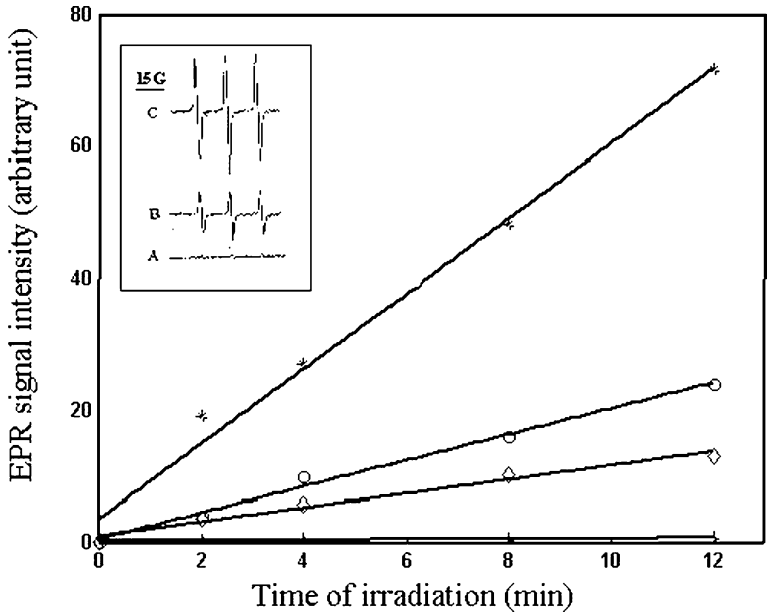


Fig. 4. The formation of TEMPOL during the photoirradiation of RB (∗), DAM (○) and NDAM (◇) in the presence of TEMPL (20 mM) at 300 K in DMSO. Inhibitory effect of 2 mM sodium azide (+) on the intensity of TEMPOL radical during photoirradiation of DAM. The inset shows the EPR spectrum of TEMPOL generated during the photoirradiation of DMSO solution of DAM (0.1 mM) in the presence of TEMPL: (A) in the dark; (B) 4 min irradiation; (C) 8 min irradiation. Spectrometer settings: microwave power, 2 mW; modulation frequency, 100 kHz; modulation amplitude, 0.5 G; time constant, 0.1 s; scan rate, 4 min; scan width, 200 G.

2 ms, inferring that this triplet is sufficient to react with oxygen even at room temperature. The $^1O_2$ quantum yield for DAM and NDAM are 0.254 and 0.104, respectively, using PN as standard ($\Phi^1O_2$ for PN = 1 in acetonitrile [33]). These values are in reasonable agreement with the values estimated by EPR-TEMPL method and RNO bleaching assay.

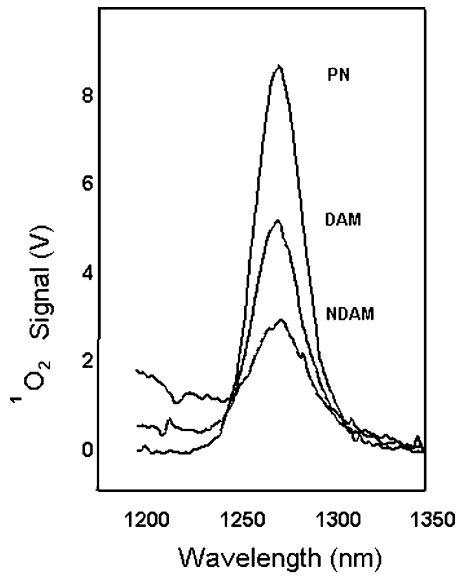


Fig. 5. Spectrum of $^1O_2$ phosphorescence of PN, DAM and NDAM in acetonitrile.

### 3.2. Generation of $O_2^{\bullet-}$

The photogeneration of $O_2^{\bullet-}$ was studied by following ferricytochrome *c* reduction [22]. The rate of photoreduction of cytochrome *c* was also studied in the presence of electron donors such as EDTA and NADH. The electron donors enhanced the rate of cytochrome *c* reduction. This is typically shown for NADH in Fig. 6. This enhancement of photogeneration of $O_2^{\bullet-}$ in the presence of electron donor is indicative of anionic properties of the radical intermediate formed during the photodynamic process [34]. In the presence of electron donors such as EDTA and NADH, the pathways of $^1O_2$ generation can effectively switch over into the production of the anionic species $S^{\bullet-}$ due to the interaction of electron donor with the triplet state of the sensitiser as shown in Scheme 1. In the presence of oxygen the electron transfer can occur from $S^{\bullet-}$ to $O_2$. The various photophysical processes are outlined in Scheme 1. Addition of SOD was found to inhibit the photoreduction, thus confirming the formation of $O_2^{\bullet-}$ upon irradiation.

DAM shows higher photogeneration efficiencies of $^1O_2$ and $O_2^{\bullet-}$, compared to NDAM. The DAM contains $–OCH_3$ group while NDAM has –OH at position-1. Electron-donating substituents directly attached to quinone ring are known to enhance their activity [35]. On this account DAM is expected to show higher efficiencies for generation of $^1O_2$ and $O_2^{\bullet-}$ than NDAM.

The photogeneration of $O_2^{\bullet-}$ was also studied by EPR spin trapping technique [36,37]. Lifetime of the spin adduct DMPO–$O_2^{\bullet-}$ is short in protic solvent and the superoxide

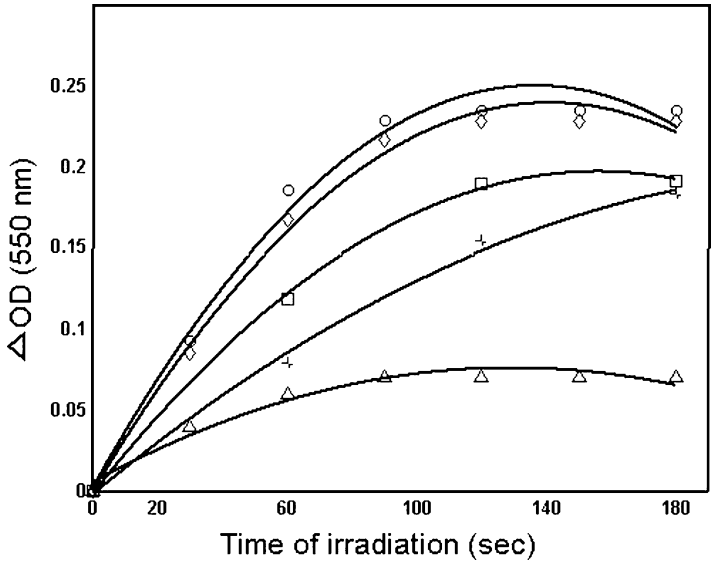


Fig. 6. Photosensitised superoxide generation measured as the rate of cytochrome *c* reduction in 50 mM phosphate buffer, pH 7.4 by DAM (□), DAM + NADH (○), NDAM (+), NDAM + NADH (◇) and DAM + SOD (△) as a function of irradiation time.

adduct decomposes to DMPO–OH [38]. Hence, EPR spin trapping studies were carried out in DMSO in which the DMPO–$O_2^{\bullet -}$ adduct has a longer life time [39]. No EPR signal was observed in dark as well as when DMPO alone was irradiated in DMSO (Fig. 7A). But the irradiation of DAM (0.2 mM) and DMPO (100 mM) in aerated DMSO generated a 12-line EPR spectrum characteristic of the DMPO–$O_2^{\bullet -}$ adduct (Fig. 7B). The identity of this radical was further confirmed by computer simulation of the spectrum (Fig. 7C). The hfcc of the spin adduct was analysed as primary nitrogen triplet ($A_N = 13.5$ G) split by a proton ($A_H^{\beta} = 10.9$ G) which in turn is further split by a secondary proton ($A_H^{\gamma} = 1.4$ G). These hfcc are consistent with DMPO–$O_2^{\bullet -}$ adduct in DMSO [40]. The signal intensity of this spin adduct was found to increase with increasing time of irradiation. Addition of SOD (50 μg/ml) prior to irradiation prevents the

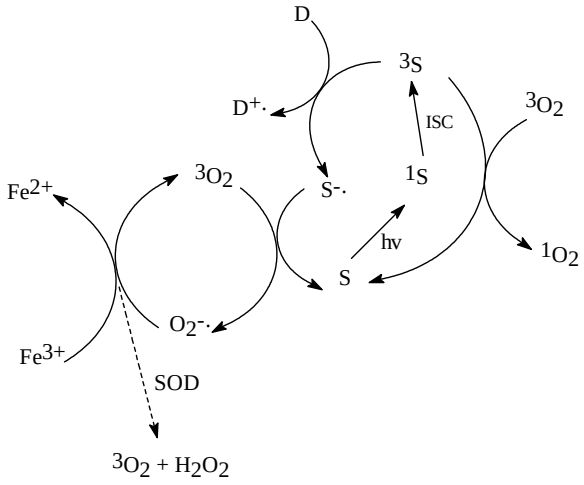


Scheme 1.

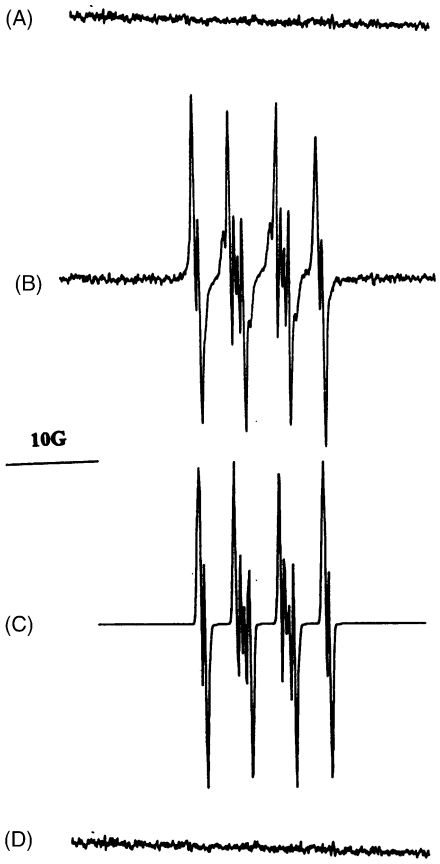


Fig. 7. EPR spectra of DMPO adduct in aerated DMSO solution containing DAM (0.2 mM) and DMPO (100 mM) (A) in dark, (B) after 4 min irradiation, (C) computed simulated EPR spectrum of DMPO–$O_2^{\bullet -}$ adduct using hfcc values $A_N = 13.5$ G, $A_H^{\beta} = 10.85$ G, $A_H^{\gamma} = 1.42$ G and (D) in the presence of SOD (50 μg/ml). Spectrometer setting: microwave power, 2 mW; modulation frequency, 100 kHz; modulation amplitude, 0.5 G; time constant, 0.1 s; scan rate, 4 min; scan width, 200 G; receiver gain, 500; line width, 1.1.

formation of adduct (Fig. 7D). NDAM also showed similar behaviour. The hfcc values evaluated for DMPO–$O_2^{\bullet-}$ adduct ($A_N = 14.3$ G, $A_H^{\beta} = 11.4$ G and $A_H^{\gamma} = 1.3$ G) and the DMPO–$CH_3$ adduct ($A_N = 16.4$ G, $A_H^{\beta} = 23.6$ G) (figure not shown). The adduct DMPO–$CH_3$ observed is possibly due to a secondary radical derived from DMSO and hydroxyl radical [41].

### 3.3. Redox potentials

Electrochemical studies were carried out to determine the reduction potentials for both DAM and NDAM. Cyclic voltammogram of the two quinones were measured in the range of +1.0 to −1.8 V. DAM and NDAM show one cathodic and one anodic peak (Fig. 8). The reduction potentials, $E_{1/2}$ for DAM and NDAM were found to be −0.815 and −0.798 V, respectively (Table 1).

The half-wave potential of DAM is more negative than that of NDAM. Electron-donating substituents are known to cause a shift of $E_{1/2}$ to more negative value [42,43]. These $E_{1/2}$ values suggest NDAM to be more readily reducible.

### 3.4. Electronic properties of DAM and NDAM

The electronic properties of DAM and NDAM have relevance to the modulation of their binding to biological targets. The detailed MO computational studies of the two structures are presented in Table 2. The two naturally occurring anthraquinones DAM and NDAM have structural difference in the side chains. The optimised structures are given in Fig. 9.

In the case of NDAM, hydrogen bonding between the aromatic OH and the quinone substituted carbonyl functions limits the side chain conformational freedom and makes the substitution coplanar with the ring system. But in the case of electron-donating substituent $OCH_3$ (DAM) the hydrogen bonding with carbonyl group is restricted and the substituent is projected out of the plan with the ring system. Total energies, highest occupied molecular orbital (HOMO) and lowest unoccupied molecular orbital (LUMO) energies and electric dipole moments, calculated for the two structures are presented in Table 2.

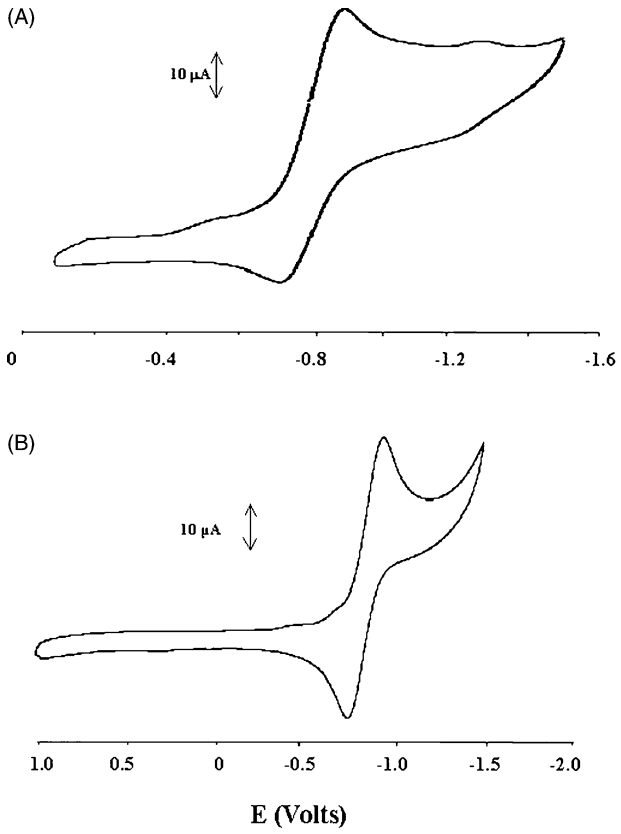


Fig. 8. Cyclic voltammograms of (A) DAM and (B) NDAM in acetonitrile containing TBAP as supporting electrolyte (0.05 M) at 100 mV/s scan rate.

Table 1
Cyclic voltammetric data[a] of DAM and NDAM

| Substrate | Peak potential (V) | | $\Delta E_p$ | $E_{1/2}$ | Peak current (μA) | | $I_{pa}/I_{pc}$ |
|---|---|---|---|---|---|---|---|
| | $E_{pc}$ | $E_{pa}$ | | | $I_{pc}$ | $I_{pa}$ | |
| DAM | −0.894 | −0.736 | 0.158 | −0.815 | 3.78 | 1.98 | 0.52 |
| NDAM | −0.885 | −0.710 | 0.175 | −0.798 | 3.32 | 2.70 | 0.81 |

[a] Potentials in volts against Ag/AgCl; scan rate, 100 mV/s.

Table 2
Total energies, frontier orbital energies and electric dipole moments for DAM and NDAM

| Compounds | $E_{1/2}$ (V) | AM1 (RHF), $\Delta H_f$ (kcal/mol) | ZINDO (RHF) | | |
|---|---|---|---|---|---|
| | | | HOMO (au)[a] | LUMO (au) | Dipole moment (debye) |
| DAM | −0.815 | −104.79 | −0.3401 | −0.0711 | 5.9992 ($x = -3.381$, $y = -4.940$, $z = -0.389$)[b] |
| NDAM | −0.798 | −117.49 | −0.3355 | −0.0741 | 5.9462 ($x = -1.613$, $y = -5.636$, $z = -0.998$)[b] |

[a] Atomic unit.
[b] Vector composition of electric dipole moment.

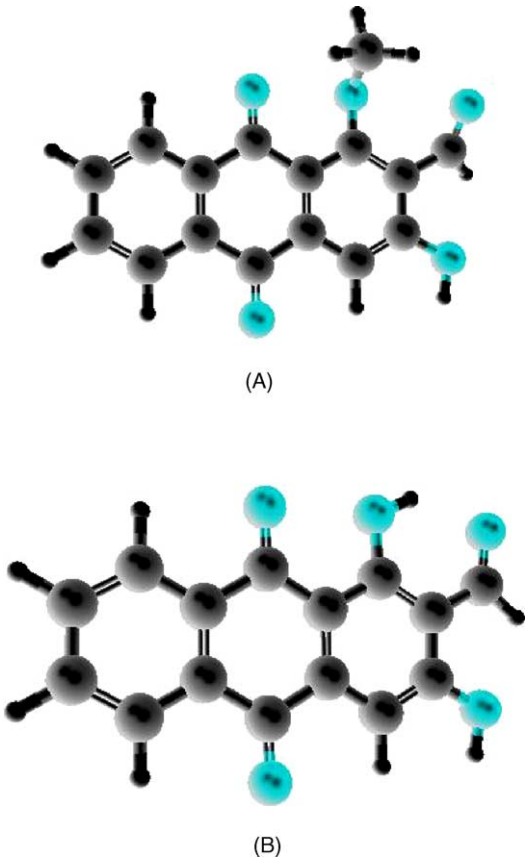


Fig. 9. AM1 (RHF) optimised structures for the models of (A) DAM and (B) NDAM.

The most prominent chemical feature of quinones is their ability to undergo redox cycling to generate ROS. Damage to tumour cell results from their ability to undergo enzymatic reduction to the semiquinone radical [44,45]. So, electron transfer plays a major role in the mechanism of action of antitumour drugs. The LUMO energies for the DAM and NDAM (Table 2) correlate well with experimental one-electron reduction potentials ($E_{1/2}$) [46]. The HOMO–LUMO energy gaps for compounds DAM and NDAM are 0.2790 and 0.2614 (au), respectively (Table 2). In general both compounds show higher value of energy gap, this indicates polarisability decreases [47]. The HOMO–LUMO energy gap is related to geometrical characteristics. The higher bandgap energy of DAM may be due to the presence of bulky substituents on C-1, that may break the coplanarity of conjugated backbone [48].

In conclusion, we provide strong evidence for both electron transfer (Type I) and $^1O_2$ energy transfer (Type II) mechanism for the photosensitisation of DAM and NDAM. The type II process is confirmed by EPR-TEMPL and chemiluminescence methods. Type I process is confirmed by SOD inhibitable cytochrome *c* reduction assay and DMPO spin trapping experiments. The structural modification in the anthraquinones DAM and NDAM are responsible for the LUMO energy differences. These LUMO energies are correlated with the experimental redox potential.

## Acknowledgements

We thank Chemistry Department, Pondicherry University, Pondicherry, for EPR measurements. Thanks are due to the UGC, New Delhi, for the award of a teacher fellowship and to the Managing Board, NMSSVN College, Madurai, Tamil Nadu, for study leave to MR. Financial assistance from UGC New Delhi (Departmental Research Support), to School of Chemistry, Madurai Kamaraj University, is gratefully acknowledged. We also thank M.A. Thompson's free trial version software Argus 3.0 available for semi-empirical quantum mechanical calculations.

## References

[1] V. Eswaran, V. Naryanan, S. Neelakantan, P.V. Raman, Indian J. Chem. 17B (1979) 650.
[2] E.M. Palsson, M. Popoff, M. Thelestam, L.A. O'Neill, J. Biol. Chem. 275 (2000) 7818.
[3] K.A. Fitzgerald, A.G. Bowie, B.S. Skeffington, L.A. O'Neill, Ras, J. Immunol. 164 (2000) 2053.
[4] A.Y. Zubkov, K.S. Rollins, A.D. Parent, J. Zhang, R.M. Bryan Jr., Stroke 31 (2000) 526.
[5] C.R. Faltynek, J. Schroeder, P. Mauvais, D. Miller, S. Wang, D. Murphy, R. Lehr, M. Kelley, A. Maycock, W. Michne, et al., Biochemistry 34 (1995) 12404.
[6] K. Aoki, A. Parent, J. Zhang, Eur. J. Pharmacol. 387 (2000) 119.
[7] L.M. Toledo, N.B. Lydon, D. Elbaum, Curr. Med. Chem. 6 (1999) 775.
[8] H. Tosa, M. Iinuma, F. Asai, T. Tanaka, H. Nozaki, S. Ikeda, K. Tsutsui, M. Yamada, S. Fujimori, Biol. Pharm. Bull. 21 (1998) 641.
[9] T. Hiwasa, Y. Arase, Z. Chen, K. Kita, K. Umezawa, H. Ito, N. Suzuki, FEBS Lett. 444 (1999) 173.
[10] B. Kalyanaraman, C.C. Felix, R.C. Sealy, Photochem. Photobiol. 36 (1982) 12.
[11] I. Kraljic, S. El Mohsni, Photochem. Photobiol. 28 (1978) 577.
[12] E. Gandin, Y. Lion, A. Van De Vorst, Photochem. Photobiol. 37 (1983) 271.
[13] E. Gandin, Y. Lion, J. Photochem. Photobiol. 30 (1982) 77.
[14] P.C.C. Lee, A.J. Rodgers, J. Photochem. Photobiol. 45 (1987) 79.
[15] J. Johnson Inbaraj, R. Gandhidasan, R. Murugesan, J. Photochem. Photobiol. A 124 (1999) 95.
[16] Y. Lion, M. Demelle, A. Van De Vorst, Nature 263 (1976) 442.
[17] J. Moan, E. Wold, Nature 279 (1979) 450.
[18] M.C. Krishna, W. DeGraff, T.S. Gonzalez, F.J. Amram Samuni, A. Russo, J.B. Mitchell, Cancer Res. 51 (1991) 6622.
[19] S.M. Hahn, L. Wilson, M.C. Krishna, J. Liebmann, W. Degraff, J. Gamson, A. Samuni, D. Venzon, J.B. Mitchell, Radiat. Res. 132 (1992) 87.
[20] R.D. Hall, C.F. Chignell, Photochem. Photobiol. 45 (1987) 459.
[21] J. Johnson Inbaraj, B.M. Kukielczak, P. Bilski, S.L. Sandvik, C.F. Chignell, Chem. Res. Toxicol. 14 (2001) 1529.
[22] J.M. Mc Cord, I. Fridovich, J. Biol. Chem. 244 (1969) 6049.
[23] W.H. Koppenol, J. Butler, Isr. J. Chem. 24 (1984) 11.
[24] Z.J. Diwu, J.W. Lown, J. Photochem. Photobiol. B 18 (1993) 131.
[25] G.R. Beuttner, L.W. Oberley, Biochem. Biophys. Res. Commun. 83 (1977) 69.
[26] M.A. Thompson, Argus 3.0, Pacific Northwest Laboratory, Richland, WA, 1994.

[27] M.J.S. Dewar, W. Thiel, J. Am. Chem. Soc. 99 (1977) 4899.
[28] M.J.S. Dewar, E.G. Zoebisch, E.F. Healy, J.J.P. Stewart, J. Am. Chem. Soc. 107 (1985) 3902.
[29] M.C. Zerner, G. Loew, R. Kirchner, V. Mueller-Westerhoff, J. Am. Chem. Soc. 102 (1980) 589.
[30] F. Wilkinson, J.G. Brummer, J. Phys. Chem. Ref. Data 10 (1981) 809.
[31] C.M. Krishna, S. Uppuluri, P. Riesz, J. Samuel Zigler Jr., D.A. Balasubramanian, Photochem. Phtobiol. 54 (1991) 51.
[32] E. Olveros, P. Suardi-Murasecco, T. Arminian-Saghaji, H.J. Hansen, Helv. Chim. Acta 74 (1991) 79.
[33] J. Johnson Inbaraj, P. Bilski, C.F. Chignell, Photochem. Photobiol. 75 (2001) 1.
[34] Z. Diwu, Free Radic. Biol. Med. 14 (1993) 209.
[35] J.S. Driscoll, G.F. Hazard Jr., H.B. Wood Jr., A. Goldin, Cancer Chemotherapy Reports, Part 2, vol. 4, 1974.
[36] T. Wu, J. Shen, A. Song, S. Chen, M. Zhang, T. Shen, Photochem. Photobiol. B 57 (2000) 14.
[37] H. Zhang, J. Joseph, J. Vasquez-Vivar, H. Karoui, C. Nsanzumuhire, P. Martasek, P. Tordo, B. Kalyanaraman, FEBS Lett. 473 (2000) 58.
[38] E. Finkelstein, G.M. Rosen, E.J. Rauckman, Mol. Pharmacol. 21 (1982) 262.
[39] E. Ben-Hur, A. Carmichael, P. Riesz, I. Rosenthal, Int. J. Radiat. Biol. 48 (1985) 837.
[40] Z. Zhiyi, M. Nenghui, W. Qian, Li Meifan. Free Radic. Biol. Med. 14 (1993) 1.
[41] S.I. Dikalov, R.P. Mason, Free Radic. Biol. Med. 27 (1999) 864.
[42] R.J. Driebergen, W. Verboom, D.N. Reinhoudt, P. Lelieveld, Anticancer Res. 6 (1986) 605.
[43] C. Hansch, A. Leo, S.H. Vnger, K.H. Kim, D. Nikaitaini, E.J. Lien, J. Med. Chem. 16 (1973) 1207.
[44] B. Kalyanaraman, K.M. Morehouse, R.P. Mason, Arch. Biochem. Biophys. 286 (1991) 164.
[45] J. Schreiber, C. Mottley, B.K. Sinha, B. Kalyanaraman, R.P. Mason, J. Am. Chem. Soc. 109 (1987) 348.
[46] G. Zagotto, S. Moro, E. Uriarte, E. Ferrazzi, G. Palu, M. Palumbo, Anti-cancer Drug Des. 12 (1997) 99.
[47] M.G. Kuzyk, C.W. Dirk, Phys. Rev. A 41 (1990) 5098.
[48] F. Naso, F. Babudri, G.M. Farinola, Pure Appl. Chem. 71 (1999) 1485.